EARTHQUAKE ENGINEERING AND STRUCTURAL DYNAMICS
Earthquake Engng Struct. Dyn. 2003; **32**:2425–2450 (DOI: 10.1002/eqe.335)

Ground motion scaling methods for different site conditions and structure characteristics

Y. C. Kurama[1,*,†], and K. T. Farrow[2]

[1] *Department of Civil Engineering and Geological Sciences, University of Notre Dame, Notre Dame, IN 46556-5637, U.S.A.*
[2] *ExxonMobil Upstream Research Co., Offshore Division, Houston, TX 77252, U.S.A.*

SUMMARY

Non-linear dynamic time-history analyses conducted as part of a performance-based seismic design approach often require that the ground motion records are scaled to a specified level of seismic intensity. Recent research has demonstrated that certain ground motion scaling methods can introduce a large scatter in the estimated seismic demands. The resulting demand estimates may be biased, leading to designs with significant uncertainty and unknown margins of safety, unless a relatively large ensemble of ground motion records is used. This paper investigates the effectiveness of seven ground motion scaling methods in reducing the scatter in estimated peak lateral displacement demands. Non-linear single-degree-of-freedom systems and non-linear multi-degree-of-freedom systems are considered with different site conditions (site soil profile and epicentral distance) and structural characteristics (yield strength, period, and hysteretic behavior). It is shown that scaling methods that work well for ground motions representative of stiff soil and far-field conditions lose their effectiveness for soft soil and near-field conditions for a wide range of structural characteristics. Copyright © 2003 John Wiley & Sons, Ltd.

KEY WORDS: ground motion scaling; hysteresis type; multi-degree-of-freedom; performance-based seismic analysis and design; single-degree-of-freedom; site conditions

INTRODUCTION

Performance-based seismic design refers to a noble concept that aims to allow the designer to specify and predict, with reasonable accuracy, the performance (degree of damage) of a structure for a specified level of ground motion intensity. This requires that non-linear dynamic time-history analyses conducted as part of a performance-based design approach use ground motion records that are scaled to adequately define the damage potential for given site conditions and structural characteristics.

* Correspondence to: Y. C. Kurama, Department of Civil Engineering and Geological Sciences, University of Notre Dame, Notre Dame, IN 46556-5637, U.S.A.
† E-mail: ykurama@nd.edu

Received 27 March 2002
Revised 28 October 2002 and 11 April 2003
Accepted 11 April 2003

The dynamic analysis procedures in current U.S. seismic design provisions [1–3] specify that a series of non-linear time-history analyses are conducted with pairs of horizontal ground motion components selected from not less than three events. If three pairs of records are used, then the maximum value of the response parameter of interest (e.g., peak lateral displacement) is taken for design. If seven or more pairs of records are used, then the mean value of the response parameter may be used for design. With the small number of ground motion records specified by current design provisions, the method used to scale these records to describe the expected seismic intensity at a site is of concern [4]. Merely, the provisions require that the mean acceleration response spectrum of the ground motion ensemble used in design is not less than 1.4 times a 5%-damped smooth design response spectrum, given by the provisions, for periods between $0.2T_o \leqslant T \leqslant 1.5T_o$, where T_o is the structure linear-elastic fundamental period. While the intent is straightforward (i.e., to match or exceed 1.4 times the smooth design spectrum), there are several methods that can be used to scale the ground motions in an ensemble to produce a mean spectrum that satisfies this requirement.

Previous research, described in more detail below, has demonstrated that certain scaling methods can result in excessive scatter in the estimated seismic demands. For example, it has been shown that scaling ground motion records based on the peak ground acceleration introduces a large scatter in the analysis results [4–7]. This indicates that the seismic demand estimates may be biased, leading to designs with significant uncertainty and unknown margins of safety, unless a relatively large number of records is used [4]. Ground motion scaling methods that minimize the scatter in the demand estimates need to be developed to minimize the number of records needed to obtain a reasonable estimate of the mean response. This is particularly important for structures that undergo large non-linear displacements, since, it has been shown that the scatter in the demand estimates increases at higher levels of non-linear behavior [8].

The research described in this paper, given in full detail in Farrow and Kurama [9], addresses this issue. It is shown that the effectiveness of ground motion scaling methods in minimizing the scatter in peak displacement demands depends on site soil characteristics, epicentral distance, structural strength, and structural period. Scaling methods that work well for stiff soil and far-field conditions may not provide good results for soft soil and near-field conditions for a wide range of structural characteristics. This paper investigates the effectiveness of seven scaling methods for this purpose.

RECENT FINDINGS ON GROUND MOTION SCALING

There are many papers that mention or explicitly address scaling of ground motion records (e.g., References [4–7, 10–24]). A comprehensive overview of this previous research is not within the scope of this paper. In a study by Nassar and Krawinkler [12] to determine relationships between the strength ratio, R (defined as the linear-elastic force demand under a ground motion, F_{elas}, divided by the yield strength of the structure, F_{y}), the peak displacement ductility demand, μ, and the structure period of vibration, T_o, the ground motions were scaled to a peak ground acceleration (PGA) of 0.4 g. A large scatter in the results was observed, particularly for large values of R. Miranda [6] performed a similar study and observed that using acceleration parameters (e.g., PGA) to scale ground

motions increases the scatter in the non-linear acceleration demand spectra at long periods.

Shome *et al.* [10] also found the scatter to be significantly large when using scaling methods based on peak ground motion characteristics. For example, the dispersion, δ, calculated as the standard deviation of the log displacement demand estimates, was as much as 0.58 for a sample size of 20 ground motions scaled to a constant *PGA*, implying that the demand estimates are subject to significant uncertainty. It was concluded that to obtain an estimate of the median (geometric mean, defined as the exponential of the arithmetic mean of the log demand estimates) response, $\hat{\Omega}$ within a certain factor, $\pm X$ (i.e., $\hat{\Omega} \pm X\hat{\Omega}$) with 95% confidence, approximately $n_{\text{eq}} = 4\delta^2/X^2$ number of ground motion records need to be used [10]. Thus, the required number of records to obtain a reasonable estimate of the median response can be significantly reduced by reducing the scatter in the demand estimates.

Shome and Cornell [4] and Shome *et al.* [10] found that seismic demand estimates are strongly correlated with the linear-elastic spectral response acceleration at the structure fundamental period, T_o, also called the spectral intensity, $S_a(T_o)$. This observation was made for SDOF and MDOF structures with two periods ($T_o = 0.25$ and 1.05 s), using ground motion ensembles with records representative of soil profile S_2 (stiff, per UBC 1994 [2]) in California having similar magnitudes (measured as the amount of strain energy released at the source of the earthquake) and similar epicentral distances from the source of the earthquake. Shome and Cornell [4] demonstrated that when the ground motion records in an ensemble are scaled up or down so that their spectral intensities at the linear-elastic structure period are equal to the median spectral intensity of the ensemble (i.e., $\hat{S}_a(T_o)$ scaling method), the scatter in the demand estimates can be significantly reduced while maintaining more or less the same median demands. Scatter can be further reduced without significantly affecting the median demands, by: (i) scaling the records based on the median spectral intensity of the ensemble over a range of structural periods [4, 10, 11, 13]; and (ii) scaling at higher levels of damping [4, 13]. These methods of scaling were found to be better methods to define the seismic damage potential for given site conditions and structural characteristics by reducing the scatter in the demand estimates.

The main contributions of the research described in this paper, in relation to the previous research described above, are to show that: (a) ground motion scaling methods based on spectral intensity measures can result in significant scatter in the estimated peak displacement demands, especially for structures designed to undergo large non-linear displacements (i.e., with large R ratios) on sites with soft soil profiles; and (b) scaling of ground motion records based on the maximum incremental velocity (*MIV*), described later, provides better results for a wide range of site conditions and structural characteristics. A large number of SDOF and MDOF dynamic time-history analyses are conducted to reinforce these findings.

DESCRIPTION OF THE ANALYTICAL PROGRAM

This section describes the analytical program as follows: (1) analytical models; (2) earthquake ground motion ensembles; (3) ground motion scaling methods; (4) dynamic time-history analyses; and (5) statistical evaluation of the demand estimates.

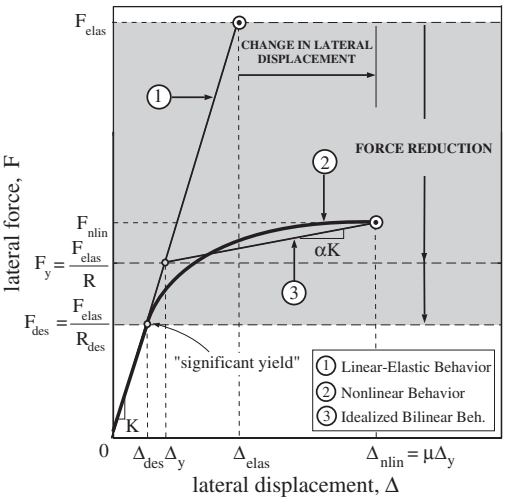

Figure 1. Lateral force-displacement relationships.

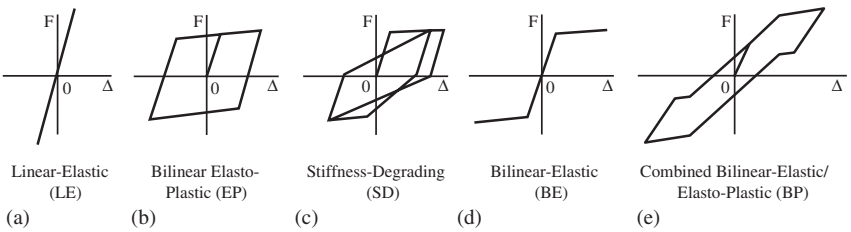

Figure 2. Hysteresis types: (a) LE; (b) EP; (c) SD; (d) BE; (e) BP.

Analytical models

Single-degree-of-freedom and multi-degree-of-freedom models are considered as described below.

Single-degree-of-freedom (SDOF) models. SDOF models with idealized bilinear force–displacement relationships, as shown in Figure 1, are used. The yield strengths, F_y, of the models are determined by dividing the linear-elastic force demands, F_{elas}, under the ground motion records used in the dynamic analyses with the strength ratio, R. Note that the definition of R in this paper is different from current seismic design provisions, which use R to specify the required design strength of a structure. The R ratio in this paper is used to quantify the yield strength, F_y, with respect to the linear-elastic force demand, F_{elas}. In this context, R is considered as a structural property and not as a code-specified constant.

Five hysteresis types are considered as illustrated in Figure 2. The importance of each type is briefly described as follows: (i) the linear-elastic (LE) type is used to determine the linear-elastic force demand, F_{elas}, under a ground motion (these analyses correspond to $R = 1$); (ii) the bilinear elasto-plastic (EP) hysteresis type represents a structure with a high level of energy dissipation and limited self-centering capability (e.g., a steel structure); (iii) the

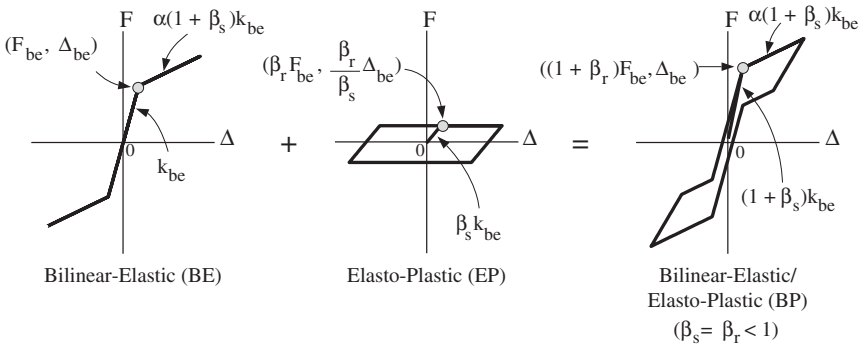

Figure 3. BP hysteresis type with $\beta_s = \beta_r < 1$.

stiffness-degrading (SD) hysteresis type is the same as the Modified Clough stiffness degrading model [25] and represents a structure with a modest level of inelastic energy dissipation and stiffness degradation due to cyclic damage (e.g., a cast-in-place reinforced concrete structure); (iv) the bilinear-elastic (BE) hysteresis type represents an idealized model for structures with little inelastic energy dissipation and a high level of self-centering capability (e.g., a post-tensioned precast concrete structure as described by Kurama [26]); and (v) the combined bilinear-elastic/elasto-plastic (BP) hysteresis type represents a structure with a modest level of inelastic energy dissipation and high self-centering capability (e.g., a post-tensioned precast concrete structure with supplemental energy dissipation as described by Kurama [26]).

The BP hysteresis type is constructed by placing the BE and EP hysteresis types in parallel. The BE type represents the primary system (e.g., precast concrete structure) and the EP type represents the secondary system (e.g., supplemental energy dissipation system). The relationships between the lateral stiffnesses and strengths of the BE and EP hysteresis types that make up a BP type are: $k_{ep} = \beta_s k_{be}$ and $F_{ep} = \beta_r F_{be}$, where k_{be} and k_{ep} are the linear-elastic stiffnesses, and F_{be} and F_{ep} are the yield strengths of the BE and EP types, respectively, and β_s and β_r are the BP type stiffness and strength ratios, respectively. The energy dissipation of the BP type can be increased by increasing β_r. In this study, β_s is set equal to $\beta_r < 1$. Such a system has only one yield point (since $\beta_s = \beta_r$) as illustrated in Figure 3 and further discussed by Farrow and Kurama [9].

Multi-degree-of-freedom (MDOF) models. Two MDOF models are considered as shown in Figure 4. These models represent four-story and eight-story cast-in-place reinforced concrete special moment-resisting frames, designed according to the UBC 1997 [2] equivalent lateral force procedure for a region with high seismicity (San Francisco bay area) and for the S_E (soft) soil profile. The frames were designed as office buildings; however, note that the span lengths of 5 m and 5.5 m may be shorter than typical span lengths in office buildings.

Both structures have identical floor plans. For each structure, an interior frame in the E–W direction (Figure 4(b)) is analyzed assuming that the floor diaphragms are sufficiently rigid under in-plane forces. The required design base shear strengths of the frames, F_{des} (V in UBC 1997), defined at first 'significant yield' (see Figure 1), were determined based on the UBC 1997 linear-elastic smooth design response spectrum with $R_{des} = 8.5$ [2]. The beams and columns were proportioned using the UBC 1997 load combinations, including gravity loads

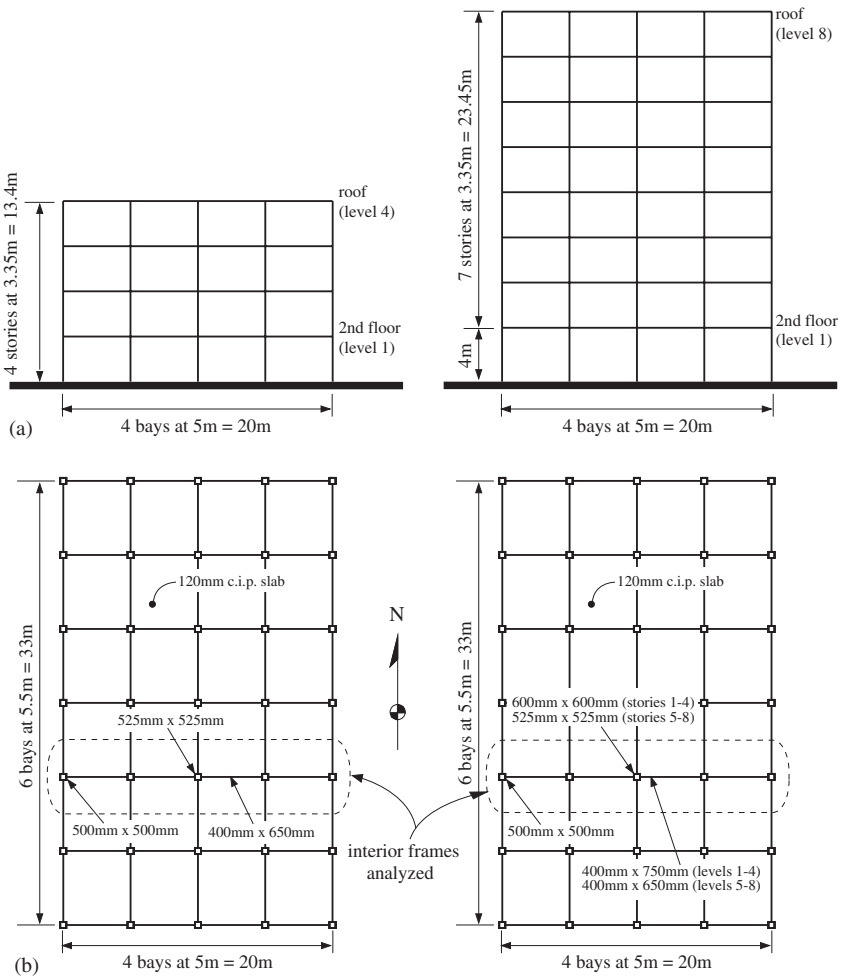

Figure 4. MDOF models: (a) elevation; (b) plan.

Table I. Frame lateral system properties.

Frame	Height (m)	Length (m)	Total frame seismic weight, W (kN)	Fundamental period, T_o (s)	Frame design base shear, F_{des} (kN)
Four-story	13.4	20	3024.8	0.49	332.7
Eight-story	27.5	20	6187.5	0.87	681.0

and earthquake-induced lateral loads [9]. Some of the design properties of the frames are provided in Table I.

A simple analytical model was developed to conduct non-linear static and non-linear dynamic time-history analyses of each frame. The columns were assumed to be fixed at the bases. The initial flexural stiffnesses of the interior columns were assumed to be 100% of

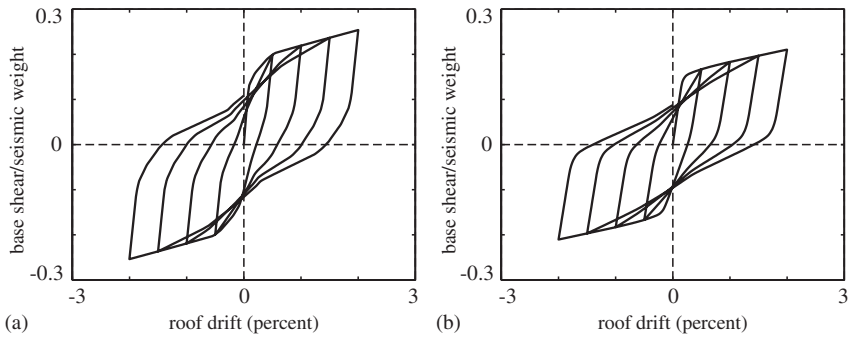

Figure 5. Normalized base shear versus roof drift behavior: (a) four-story frame; (b) eight-story frame.

the gross-section linear-elastic flexural stiffnesses. The initial 'effective' flexural stiffnesses of the exterior columns and the floor and roof beams were assumed to be 80% and 30% of the gross-section linear-elastic flexural stiffnesses, respectively, to account for cracking in the members. A T-beam flange width of 1/8 the center-to-center span length of the beam was included in the modeling of the beams [27]. The beams and columns were modeled using linear-elastic beam–column elements in the structural analysis program, DRAIN-2DX [28]. Full depth rigid end zones were assumed at the beam–column joints.

Non-linear behavior at the beam ends and in the beam–column joints was modeled as concentrated plastic hinges at the beam–column joints using zero-length rotational spring elements with stiffness degrading properties [29]. The yield moment capacities of the springs were set equal to the design beam moment demands, ignoring overstrength. The post-yield moment-rotation stiffness of the springs was determined based on a post-yield moment-curvature stiffness equal to 2% of the initial stiffness in the plastic hinge length (assumed to be equal to 1.5 times the beam depth).

In order to have a relatively simple analytical model, yielding in the columns other than at the bases was ignored. Note that column yielding at locations other than the base may be possible; however, this was not considered. Non-linear behavior at the column bases was modeled using fiber beam–column elements to account for axial–flexural interaction [28]. The frames were assumed to be adequately designed and detailed to achieve ductile behavior. P–Δ effects were included in the model.

The normalized (with respect to the seismic weight, W) base shear versus roof drift behavior of the frames under combined gravity and cyclic lateral loading is shown in Figure 5. The roof drift is equal to the roof lateral displacement divided by the structure height. For the analyses of the frames other than the analyses used in design, the gravity load was assumed to be 100% of the design dead load plus 25% of the design live load, with no live load reduction. The lateral load distribution over the height of the frames was taken as the UBC 1997 equivalent lateral force pattern [2].

Additional information on the design and modeling of the frames can be found in Farrow and Kurama [9]. Note that it may be possible to develop more accurate analytical models for the frames; however, this was not done to keep the computational time for the dynamic analyses manageable.

Ground motion ensembles

Ground motion records for sites with very dense (S_C), stiff (S_D), and soft (S_E) soil profiles were collected at the University of Notre Dame (UND) to investigate the effect of site soil characteristics on scaling [9]. The S_C, S_D, and S_E soil profiles correspond to site classes C, D, and E in IBC 2000 [1], respectively. Twenty ground motion records are used for each soil profile. In addition, twenty records representative of near-field (NF) conditions with a stiff (S_D) soil profile, compiled by the SAC steel project [30], are used to investigate the effect of epicentral distance. A total of 40 recorded horizontal motions for seismic hazard in Zone 4 and for return periods of 10% in 50 years (i.e., design level) were compiled by SAC (records NF01-NF40). The 20 odd numbered records are used in this study.

The linear-elastic SDOF pseudo-acceleration and -velocity response spectra of the ground motions with a viscous damping ratio of $\xi = 5\%$ are shown in Figure 6. The acceleration time-history records, 80 in all, were obtained from the National Geophysical Data Center archive, the Multidisciplinary Center for Earthquake Engineering Research database, Kurama *et al.* [31], and the SAC steel project [30]. The strong motion duration for each record (D_{sm}) was determined by the root mean square acceleration method [32].

Scaling methods

Seven ground motion scaling methods are investigated as follows:

(1) Peak ground acceleration ($\overline{PGA}$): each ground motion record is scaled to the arithmetic mean PGA of the ground motion ensemble.

(2) Effective peak acceleration ($\overline{EPA}$): each ground motion record is scaled to the arithmetic mean EPA of the ground motion ensemble. According to NEHRP 1994 [33], EPA is calculated as the mean linear-elastic 5%-damped spectral acceleration for the period range of 0.1 to 0.5 s divided by 2.5. The 2.5 coefficient relates back to the formulation of the design response spectra in ATC 3-06 [34].

(3) Arias intensity-based parameter ($\bar{A}_{95}$): each ground motion record is scaled to the arithmetic mean A_{95} of the ground motion ensemble. The A_{95} is defined by Sarma and Yang [35] as the acceleration that contains 95% of the Arias Intensity, $E_s = \int_0^t a^2(t)\,dt$ [14], where $a(t)$ is the acceleration time-history of the ground motion. For a given acceleration A, the area bounded by the function $a^2(t)$ and the horizontal line corresponding to A^2 is defined as E_x [35]. For example, $E_x = E_s$ for $A = 0$ and $E_x = 0$ for $A = PGA$. The acceleration that corresponds to $E_x = 0.05E_s$ is defined as A_{95}. Based on a linear regression study, Sarma and Yang [35] showed that the A_{95} parameter can be approximately determined as $A_{95} = 0.764E_s^{0.438}$, independent of the source characteristics, source size, site characteristics, and the process of correction. This approximate definition of A_{95} is used in this paper.

(4) Effective peak velocity ($\overline{EPV}$): each ground motion is scaled to the arithmetic mean EPV of the ensemble. According to NEHRP [33], EPV is equal to the linear-elastic 5%-damped spectral pseudo-velocity at period, $T = 1$ s. In this research, the EPV values of the records were calculated as the mean pseudo-velocity for periods between 0.8 and 1.2 s as recommended by Kurama *et al.* [31].

(5) Maximum incremental velocity ($\overline{MIV}$): each ground motion is scaled to the arithmetic mean MIV of the ground motion ensemble. Incremental velocity, IV, is the area under the acceleration time-history of a ground motion between two consecutive zero acceleration crossings. The maximum IV (i.e., MIV) may be a better indicator of the damage potential of a

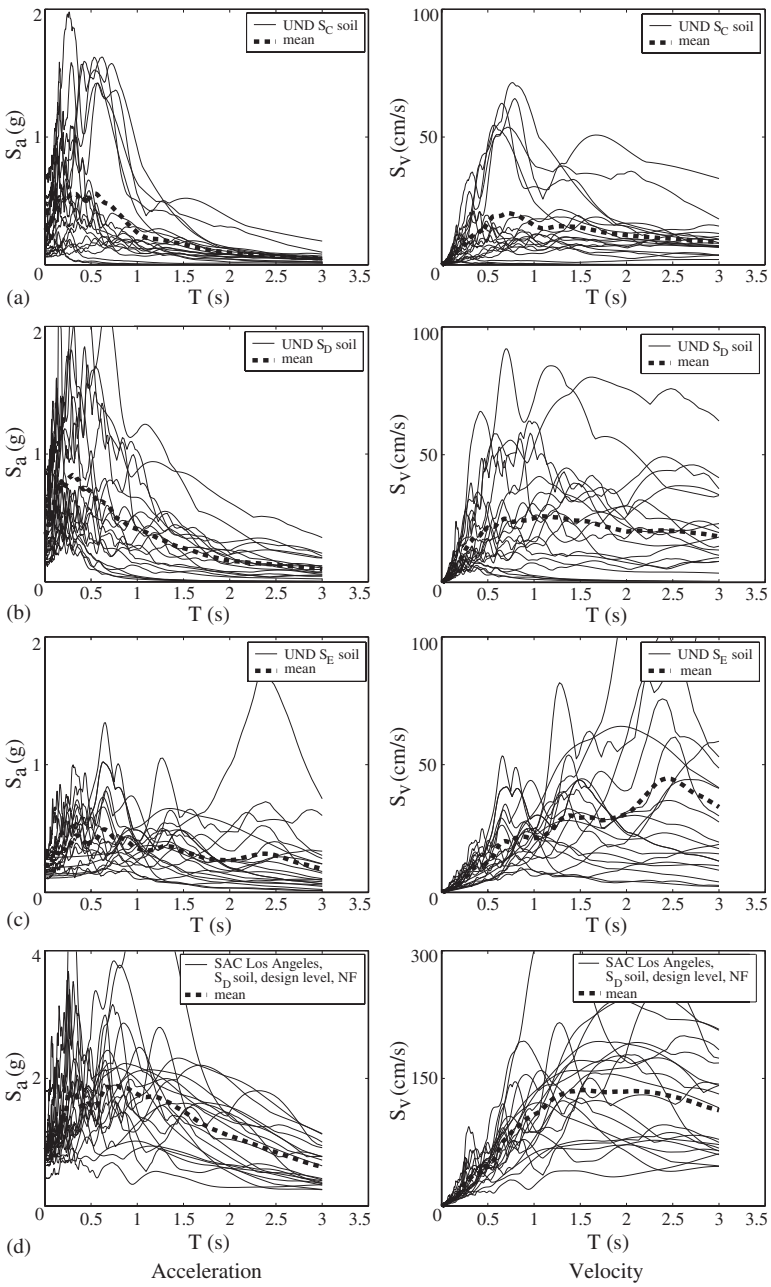

Figure 6. Response spectra ($\xi = 5\%$): (a) UND S_C soil; (b) UND S_D soil; (c) UND S_E soil; (d) SAC S_D soil, NF.

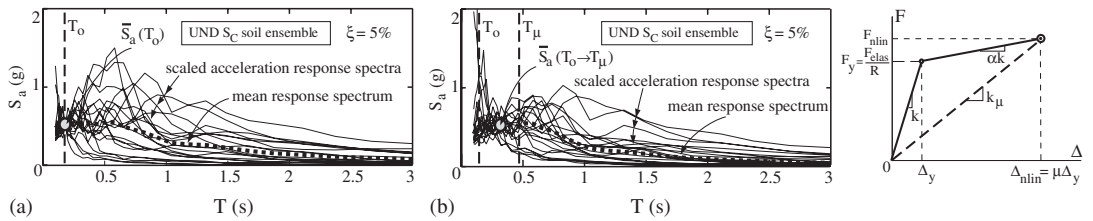

Figure 7. Scaling based on spectral acceleration: (a) $\bar{S}_a(T_o)$ method; (b) $\bar{S}_a(T_o \to T_\mu)$ method.

ground motion than *PGA* since it captures the impulsive characteristics of the ground motion [31, 36–39].

(6) Spectral response acceleration at the structure fundamental period ($\bar{S}_a(T_o)$): each ground motion is scaled to the arithmetic mean linear-elastic 5%-damped spectral acceleration of the ground motion ensemble at the linear-elastic fundamental period of the structure being analyzed, $S_a(T_o)$. Different from the scaling methods above, the $\bar{S}_a(T_o)$ method depends on the structural properties (i.e., T_o) as well as the ground motion characteristics. For example, if the structural period $T_o = 0.18$ s, each ground motion is scaled such that the spectral acceleration at 0.18 s is equal to the mean spectral acceleration, $\bar{S}_a(T_o)$, of the ensemble at 0.18 s as illustrated in Figure 7(a). The $S_a(T_o)$ parameter is also referred to as the structure-specific ground motion spectral intensity [4].

(7) Spectral acceleration over a range of structure periods ($\bar{S}_a(T_o \to T_\mu)$): each ground motion is scaled to the arithmetic mean linear-elastic 5%-damped spectral acceleration of the ground motion ensemble over a range of structural periods [4, 10, 11, 13]. First, the mean spectral acceleration, $\bar{S}_a(T_o \to T_\mu)$, of the ensemble over the period range $T_o \to T_\mu$ is calculated. Then, the records are scaled such that the mean spectral acceleration of each ground motion over the period range $T_o \to T_\mu$ is equal to $\bar{S}_a(T_o \to T_\mu)$ (see Figure 7(b)). This scaling method takes into account the elongation of the structural period due to non-linear behavior. In this research, the elongated period, T_μ, was calculated based on the secant stiffness, k_μ, corresponding to the peak displacement demand, Δ_{nlin}, as (Figure 7(b)):

$$T_\mu = T_o\sqrt{\frac{\mu}{\alpha\mu + 1 - \alpha}} \tag{1}$$

The peak displacement ductility demand, μ, can be estimated as a function of R, T_o, and α using existing relationships. A relationship by Nassar and Krawinkler [12] was used as follows:

$$R(\mu, T_o, \alpha) = [c(\mu - 1) + 1]^{1/c}, \text{ where } \mu = \Delta_{\text{nlin}}/\Delta_{\text{y}} \text{ and } c(T_o, \alpha) = \frac{T_o^a}{T_o^a + 1} + \frac{b}{T_o} \tag{2}$$

Note that the a and b coefficients in Equation (2) were developed by Nassar and Krawinkler [12] using non-linear regression based on seismic demand estimates for the EP and SD hysteresis types subjected to far-field ground motions recorded at sites representative of the S_C soil profile. These coefficients may not be applicable for other hysteresis types and/or site conditions [6, 40]. Thus, new a and b coefficients were developed in this study for the UND S_C, S_D, and S_E soil ground motions and the SAC near-field (NF) ground motions, and for the

Table II. Coefficients for R-μ-T_o relationship.

Ground motion ensemble	EP type ($\alpha = 0.10$)		SD type ($\alpha = 0.10$)		BE type ($\alpha = 0.10$)		BP type ($\alpha = 0.10$, $\beta_s = \beta_r = 1/3$)	
	a	b	a	b	a	b	a	b
UND S_C soil	1.46	0.58	–	–	–	–	–	–
UND S_D soil	1.49	0.46	1.60	0.50	2.74	0.76	2.33	0.66
UND S_E soil	−0.41	0.95	–	–	–	–	–	–
SAC NF	0.35	0.89	–	–	–	–	–	–

EP, SD, BE, and BP hysteresis types using non-linear regression analyses similar to Nassar and Krawinkler [12]. These new coefficients are given in Table II.

Dynamic time-history analyses

The SDOF and MDOF dynamic time-history analyses are described below.

SDOF analyses. A MATLAB [41] algorithm, CDSPEC (Capacity-Demand SPECtra), was developed [42] to conduct non-linear dynamic time-history analyses of the SDOF models. An incremental step-by-step formulation was used assuming that the acceleration varies linearly between the time discretization points [43]. The error tolerance and initial time step, t_s, were set as 1 per cent error in displacement and $t_s = T_o/50$, respectively. The time step was reduced in subsequent analyses until the change of displacement from the previous analysis to the current analysis was less than 1 per cent of the previous displacement. Analytical verification of the CDSPEC program is given by Farrow and Kurama [9].

The SDOF analyses were conducted using: (i) four ground motion ensembles described earlier; (ii) five strength ratios, $R = 1$ (linear-elastic), 2, 4, 6, and 8; (iii) five hysteresis types (LE, EP, SD, BE, and BP); (iv) one post-yield stiffness ratio, $\alpha = 0.10$; (v) one BP stiffness and strength ratio, $\beta_s = \beta_r = 1/3$; (vi) thirty structure periods, exponentially spaced, ranging from $T_o = 0.1$ to 3.0 s; and (vii) seven ground motion scaling methods. In all, 147 000 SDOF dynamic analyses were conducted from combinations of these parameters. The viscous damping ratio was assumed to be equal to $\xi = 5\%$.

MDOF analyses. The MDOF non-linear dynamic time-history analyses were conducted using the DRAIN-2DX program [28]. A total of 80 analyses were conducted to reinforce the findings from the SDOF analyses. The UND soft (S_E) soil ground motion ensemble was used to excite the MDOF structures in Figure 4. The ground motions were first scaled using the $\overline{MIV}$ method or the $\bar{S}_a(T_o \to T_\mu)$ method. Then, the entire ground motion ensemble was scaled for a second time by a single factor so that the mean linear-elastic acceleration response spectrum of the ensemble was not less than 1.4 times the 5%-damped UBC 1997 response spectrum used in the design of the MDOF structures for periods between $0.2T_o$ and $1.5T_o$ (where T_o is the structural fundamental period, see Table I), as required by UBC 1997 [2]. For simplicity, the scaling factors for the eight-story structure were used for both structures (the scaling factors for the $\overline{MIV}$-scaled and $\bar{S}_a(T_o \to T_\mu)$-scaled records were 3.19 and 4.11, respectively). An equivalent SDOF representation [44, 45] based on the first (fundamental) mode response,

together with Equations (1) and (2), was used in the determination of T_μ for the MDOF structures.

Rayleigh damping of $\xi = 5\%$ was assumed in the first and second vibrational modes of the four-story structure and in the first and third modes of the eight-story structure. The seismic mass of each frame was lumped at the beam–column joint nodal degrees of freedom in the horizontal direction based on tributary areas. Gravity loading of 100% of the design dead load plus 25% of the unreduced design live load was applied. P–Δ effects were considered.

Statistical evaluation of the demand estimates

The statistical evaluation of the SDOF and MDOF demand estimates is described below.

SDOF demand estimates. The effect of ground motion scaling on the scatter in the SDOF demand estimates is investigated using the dimensional peak displacement demand, Δ_{nlin}, and the non-dimensional peak displacement ductility demand, $\mu = \Delta_{\text{nlin}}/\Delta_{\text{y}}$. The results are presented as dispersion spectra corresponding to different R values by calculating the coefficient of variation, COV, defined as the ratio between the sample standard deviation, σ, and the sample mean. This measure is used to assess the effectiveness of the scaling methods in reducing the scatter in the demand estimates.

MDOF demand estimates. The evaluation of scatter in the MDOF demands is presented as response profiles of: (1) peak lateral displacement demands at floor and roof levels, Δ_i; and (2) peak interstory drift demands, $\theta_i = (\Delta_i - \Delta_{i-1})/(h_i - h_{i-1})$, where, $h_i =$ height at level i from the ground. Additionally, the results are presented as dispersions by calculating the COV of Δ_i and θ_i for the $\overline{MIV}$ and $\bar{S}_a(T_o \rightarrow T_\mu)$ scaling methods.

RESULTS OF STUDY

This section compares the seven ground motion scaling methods described earlier based on the scatter in the results from the SDOF and MDOF dynamic analyses. The SDOF results are discussed first. Then, the most important findings from the SDOF analyses are reinforced using the MDOF results. The evaluation of scatter is presented as: (i) COV-spectra; and (ii) γ-spectra, defined as the ratio of the COV-spectra for two different scaling methods.

Effect of scaling method on scatter

Figure 8 shows the scatter in the peak displacement demand, Δ_{nlin}, using the results from the UND S_D soil ground motion ensemble for the EP hysteresis type with $\alpha = 0.10$. The COV-spectra are presented on the left side of Figure 8. The solid lines in the COV-spectra represent results from the ground motions scaled to the mean peak ground acceleration (i.e., $\overline{PGA}$ scaling method) while the dashed lines represent results for the other scaling methods. The γ-spectra are on the right side of Figure 8.

For the $\overline{PGA}$, $\overline{EPA}$, and $\bar{A}_{95}$ scaling methods, the scatter tends to increase as the period T increases, similar to previous investigations [6, 7]. This is expected since these scaling methods control the short-period range of the ground motion acceleration response spectra.

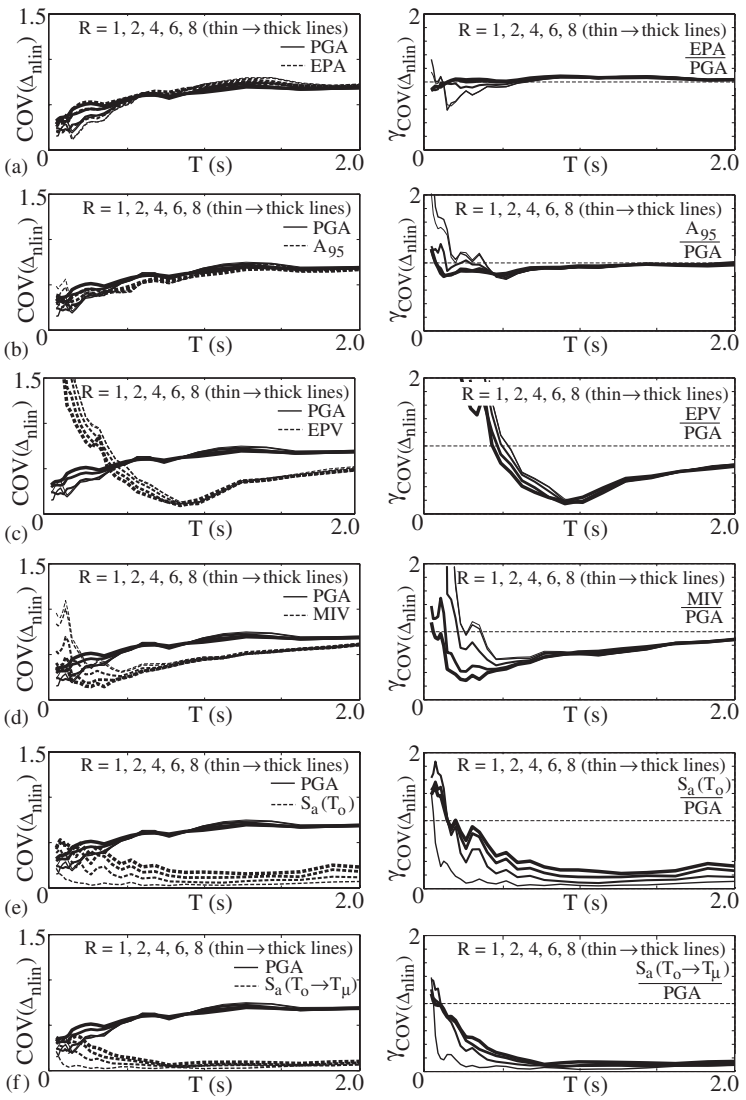

Figure 8. Scatter in Δ_{nlin} for the UND S_D soil ensemble (EP type, $\alpha = 0.10$)—$\overline{PGA}$ method compared to: (a) $\overline{EPA}$; (b) $\bar{A}_{95}$; (c) $\overline{EPV}$; (d) $\overline{MIV}$; (e) $\bar{S}_a(T_o)$; (f) $\bar{S}_a(T_o \to T_\mu)$ methods.

Overall, the differences between these three scaling methods are negligible, except for short-period structures with small R.

As compared to the $\overline{PGA}$ method, the $\overline{EPV}$ method is, on average, considerably more effective in reducing the scatter for $T > \sim 0.5$ s (Figure 8(c)). The effectiveness of the $\overline{EPV}$ method in reducing scatter is greatest at around $T = 1$ s since this method scales the ground motions to the mean spectral pseudo-velocity at around a period of 1 s. The results are relatively independent of the R ratio.

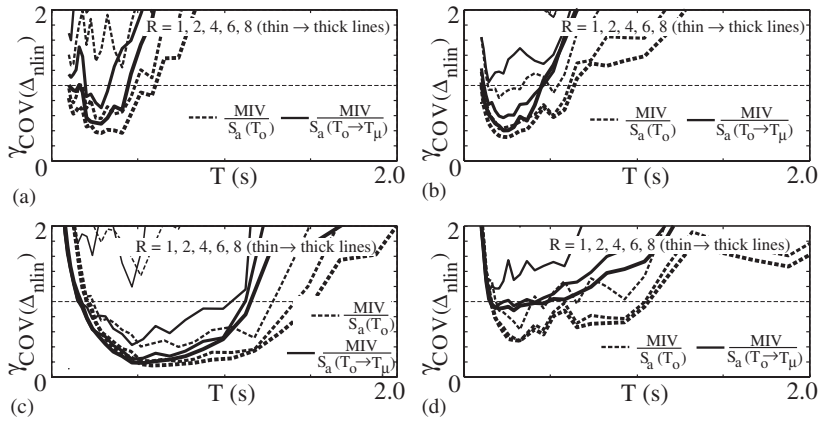

Figure 9. Scatter in Δ_{nlin} using the $\bar{S}_a(T_o)$ and $\bar{S}_a(T_o \rightarrow T_\mu)$ methods compared to the $\overline{MIV}$ method (EP type, $\alpha = 0.10$): (a) UND S_D soil; (b) UND S_C soil; (c) UND S_E soil; (d) SAC S_D soil, NF.

The $\overline{PGA}$ method is compared to scaling the ground motion ensemble to the mean maximum incremental velocity (i.e., $\overline{MIV}$ scaling method) in Figure 8(d). The results indicate that for $T > \sim 0.5$ s, the $\overline{MIV}$ method is more effective than the $\overline{PGA}$ method in reducing the scatter, independent of the R ratio. The scatter for the $\overline{MIV}$ method approaches the scatter for the $\overline{PGA}$ method as T increases. For $T < \sim 0.5$ s, the effectiveness of the $\overline{MIV}$ method decreases as R decreases.

The $\overline{PGA}$ method is compared to scaling the ground motion ensemble to the mean spectral intensity at each linear-elastic structure period (i.e., $\bar{S}_a(T_o)$ method) in Figure 8(e) and to scaling the ground motion ensemble to the mean spectral intensity over a range of structural periods (i.e., $\bar{S}_a(T_o \rightarrow T_\mu)$ method) in Figure 8(f). It can be expected that all three methods produce similar scatter for extremely short period structures since, at $T = 0$ s, the $\bar{S}_a(T_o)$ and $\bar{S}_a(T_o \rightarrow T_\mu)$ methods are equivalent to the $\overline{PGA}$ method. Also, for $R = 1$ (linear-elastic behavior), the scatter for the $\bar{S}_a(T_o)$ and $\bar{S}_a(T_o \rightarrow T_\mu)$ methods is zero for the entire period range since the ground motion records are scaled to a constant linear-elastic spectral acceleration at each linear-elastic structure period.

Unlike the $\overline{PGA}$ method, which is relatively independent of R, the COV-spectra for the $\bar{S}_a(T_o)$ method increase as R increases. With an increase in R, μ increases and, in turn, the effective structure period, T_μ, increases (see Equation (1)). Therefore, the effectiveness of the $\bar{S}_a(T_o)$ method, based on the linear-elastic structure period, T_o, decreases for larger R. Since the $\bar{S}_a(T_o \rightarrow T_\mu)$ method accounts for the period elongation due to the non-linear behavior expected in the structure, the scatter is markedly reduced and is less dependent on R, especially for $T > \sim 0.75$ s. For $T < \sim 0.75$ s, the effectiveness of the $\bar{S}_a(T_o \rightarrow T_\mu)$ method tends to decrease as R increases and T decreases.

Comparing the results for the $\bar{S}_a(T_o \rightarrow T_\mu)$ and $\overline{MIV}$ methods (solid lines, Figure 9(a)), the $\overline{MIV}$ method is more effective for $\sim 0.20 < T < \sim 0.33$s with $R = 6$ and for $\sim 0.10 < T < \sim 0.44$s with $R = 8$. Similarly, when compared to the $\bar{S}_a(T_o)$ method (dashed lines), the $\overline{MIV}$ method is more effective for $\sim 0.10 < T < \sim 0.49$s with $R = 6$ and for $\sim 0.10 < T < \sim 0.60$s with $R = 8$. Thus, it is evident that scaling ground motion records based on spectral intensity measures

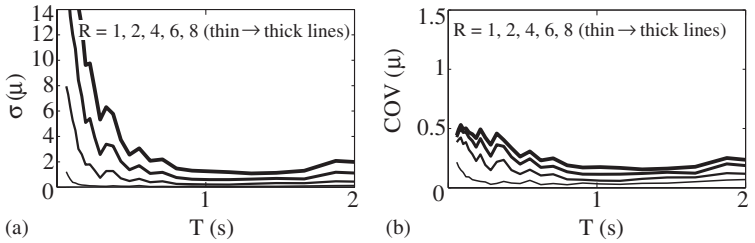

Figure 10. Scatter in μ (UND S_D soil ensemble, EP type, $\alpha = 0.10$): (a) σ; (b) COV.

(i.e., $S_a(T_o)$ and $S_a(T_o \to T_\mu)$) is not necessarily effective for all structural period ranges and strength levels. This finding is more prominent for the soft (S_E) soil ground motion ensemble (Figure 9(c)), discussed in detail later.

It was previously reported by Nassar and Krawinkler [12] that the scatter in the peak displacement ductility demand, μ, tends to increase with R. Inspecting the standard deviation, σ, for the μ-spectra (Figure 10(a)), it is evident that the scatter in μ does increase as R increases. This increase is especially significant for $T < \sim 0.75$ s. However, using the standard deviation alone as a measure of scatter can be misleading. The coefficient of variation, COV, which normalizes the sample standard deviation by the mean, is a better measure to evaluate scatter. As illustrated in Figure 10(b), the scatter in μ relative to the sample mean (i.e., COV) does not increase with R as much as the sample standard deviation, σ, especially for $T < \sim 0.75$ s (Figure 10(a)).

It should be noted that the scatter in the displacement ductility demand, $\mu = \Delta_{\text{nlin}}/\Delta_y$, is not affected by scaling when the structure yield strength, $F_y = F_{\text{elas}}/R$, is recalculated based on the acceleration response spectrum of each ground motion used in an ensemble [12]. This is because, scaling a ground motion by a constant factor equally affects both the linear-elastic force demand, F_{elas}, and the yield strength, F_y, (for a given R) resulting in the same μ. Thus, the scatter in μ shown in Figure 10 is the same for all seven scaling methods considered.

Note also that for the $\bar{S}_a(T_o)$ scaling method, the scatter in Δ_{nlin} in Figure 8(e) is the same as the scatter in μ in Figure 10(b). This is because, corresponding to a given strength ratio R and period T, the yield displacement Δ_y remains the same regardless of the ground motion used since all ground motions are scaled to the same linear-elastic spectral acceleration. For the other scaling methods considered, the scatter in Δ_{nlin} is not the same as the scatter in μ since Δ_y changes with each ground motion.

Effect of hysteresis type on scatter

The effect of the structure hysteresis type on the scatter from the different scaling methods is examined in this section. The COV-spectra for the scatter in Δ_{nlin} using the seven scaling methods are presented as is done in the previous section for the EP hysteresis type. The SD, BE, and BP hysteresis type trends (with $\alpha = 0.10$, $\beta_s = \beta_r = 1/3$), provided in Figure 11, are almost identical to the trends for the EP type in Figure 8. The γ-spectra (not shown) for the scatter in Δ_{nlin} between the different hysteresis types range from 1 to 1.25. The γ-spectra for the scatter in μ between the hysteresis types have similar values as the γ-spectra for the

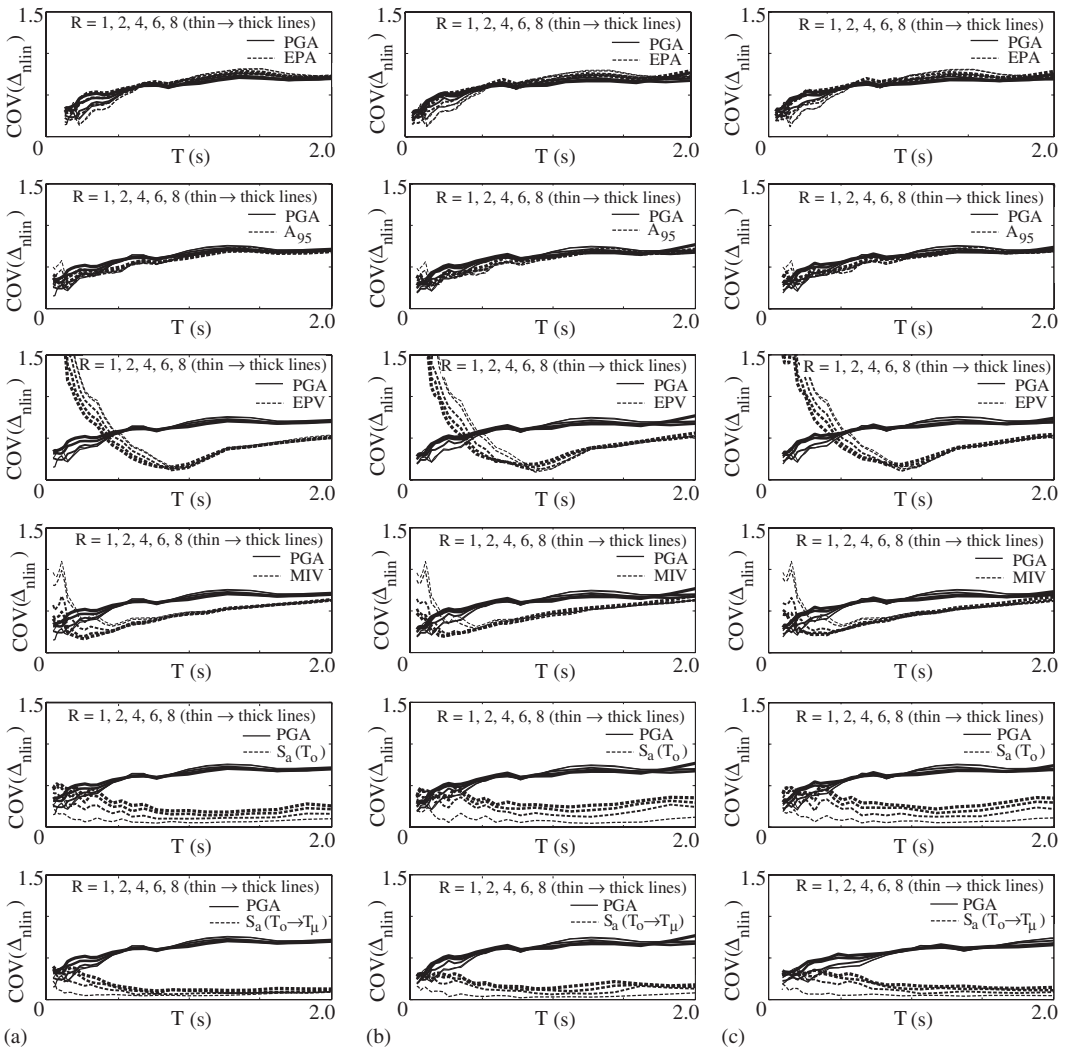

Figure 11. Effect of hysteresis type on the scatter in Δ_{nlin} (UND S_D soil ensemble, $\alpha = 0.10$): (a) SD type; (b) BE type; (c) BP type ($\beta_s = \beta_r = 1/3$).

scatter in Δ_{nlin}. Thus, it is concluded that the scatter in Δ_{nlin} and the scatter in μ are not significantly affected by the structure hysteresis type.

Effect of site soil characteristics on scatter

The effect of site soil characteristics on the scatter from the different scaling methods is examined in this section. Figures 12 and 13 show the COV-spectra for the scatter in Δ_{nlin} using the UND S_C and S_E soil ground motion ensembles, respectively, for the EP hysteresis type with $\alpha = 0.10$. Comparing Figures 8 and 12, the trends for the S_C soil ensemble are

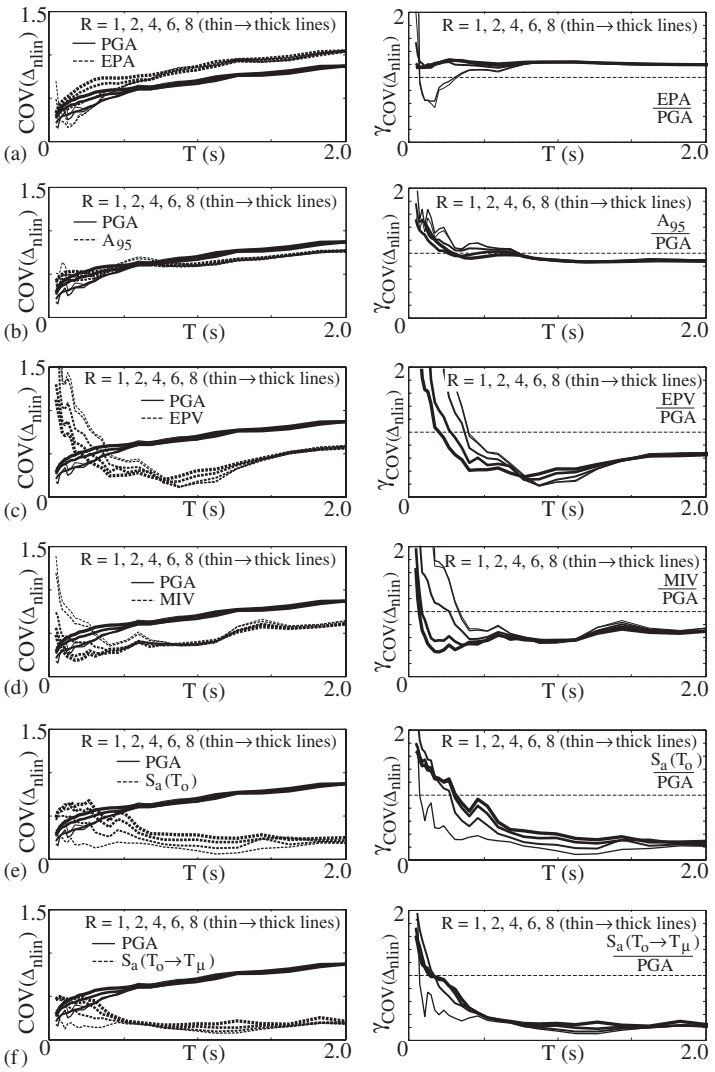

Figure 12. Scatter in Δ_{nlin} for the UND S_C soil ensemble (EP type, $\alpha = 0.10$)—$\overline{PGA}$ method compared to: (a) $\overline{EPA}$; (b) $\bar{A}_{95}$; (c) $\overline{EPV}$; (d) $\overline{MIV}$; (e) $\bar{S}_a(T_o)$; (f) $\bar{S}_a(T_o \to T_\mu)$ methods.

similar to the trends for the S_D soil ensemble. The S_C soil ensemble exhibits slightly more scatter than the S_D soil ensemble for almost the entire period range, except for the $\overline{EPV}$ and $\overline{MIV}$ methods. For the $\overline{EPV}$ method, the scatter from the S_C soil ensemble is less than the scatter from the S_D soil ensemble for $T < \sim 0.5$ s and is similar to that from the S_D soil ensemble for $T > \sim 0.5$ s. For the $\overline{MIV}$ method, the scatter from the S_C soil ensemble is similar to that from the S_D soil ensemble for the entire period range.

Comparing Figures 8, 12, and 13, the trends for the S_E soil ensemble are significantly different than the trends for the S_C and S_D soil ensembles. The S_E soil ensemble exhibits

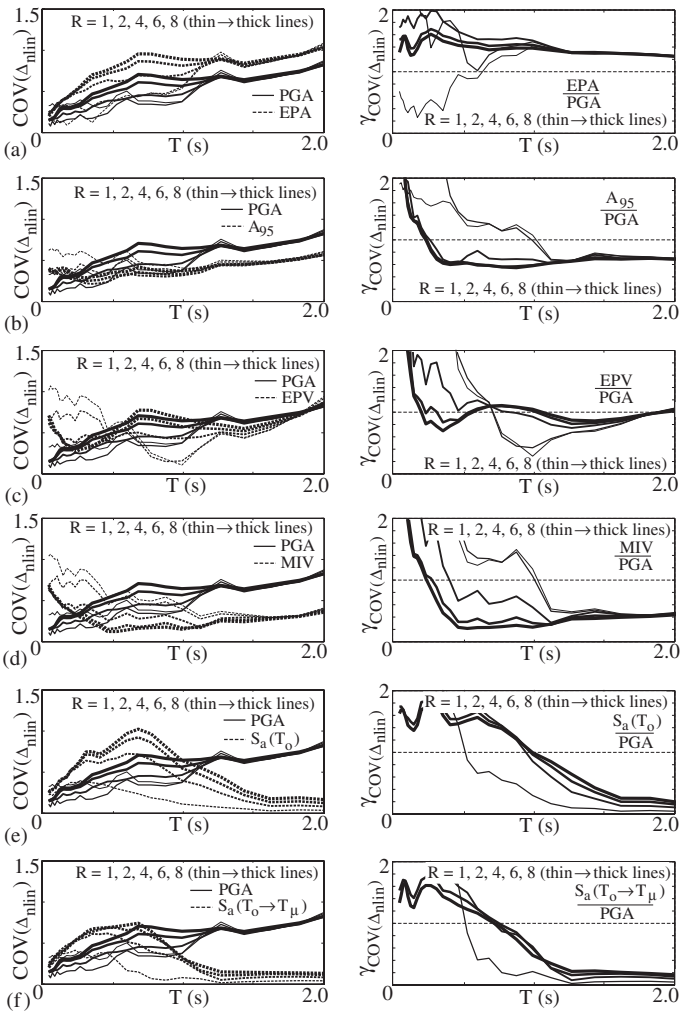

Figure 13. Scatter in Δ_{nlin} for the UND S_E soil ensemble (EP type, $\alpha = 0.10$)—$\overline{PGA}$ method compared to: (a) $\overline{EPA}$; (b) $\bar{A}_{95}$; (c) $\overline{EPV}$; (d) $\overline{MIV}$; (e) $\bar{S}_a(T_o)$; (f) $\bar{S}_a(T_o \to T_\mu)$ methods.

larger scatter for almost the entire period range, except for the $\overline{PGA}$, $\bar{A}_{95}$, and $\overline{MIV}$ methods. For $T < \sim 1.1$–1.5s, the dependency of scatter on R is significantly larger for the S_E soil profile than for the S_C and S_D soil profiles. The scatter tends to increase as R increases, except for the $\bar{A}_{95}$, $\overline{EPV}$ (with $T < \sim 0.7$ s), and $\overline{MIV}$ methods.

Figures 13(e) and (f) show that the effectiveness of the $\bar{S}_a(T_o)$ and $\bar{S}_a(T_o \to T_\mu)$ methods significantly decreases as the period decreases within the ranges of $\sim 0.75 < T < \sim 1.5$ s and $\sim 0.75 < T < \sim 1.25$ s, respectively. Note that, as stated earlier, the a and b regression coefficients used in the estimation of the effective structure period, T_μ, for the $\bar{S}_a(T_o \to T_\mu)$ method take into account site soil characteristics [9]. Even so, the scatter in the demand

estimates for $T < \sim 0.75$ s using the $\bar{S}_a(T_o \to T_\mu)$ method is larger than the scatter using the $\overline{PGA}$ method for $R = 4$, 6, and 8.

Comparing the scatter for the $\bar{S}_a(T_o \to T_\mu)$ method and the $\overline{MIV}$ method, it can be seen that the $\overline{MIV}$ method is more effective for $\sim 0.10 < T < \sim 0.46$ s with $R = 6$ and 8 for the S_C soil ground motion ensemble (Figure 9(b)) and for $\sim 0.20 < T < \sim 1.1$–1.2 s with $R = 4$, 6, and 8 for the S_E soil ensemble (Figure 9(c)). As expected, the $\overline{MIV}$ method is even more effective when compared to the $\bar{S}_a(T_o)$ method for $\sim 0.10 < T < \sim 0.64$ s with $R = 6$ and 8 for the S_C soil ensemble and for $\sim 0.20 < T < \sim 1.3$–1.5 s with $R = 4$, 6, and 8 for the S_E soil ensemble. The reduction in the scatter when using the $\overline{MIV}$ method as compared to the $\bar{S}_a(T_o)$ and $\bar{S}_a(T_o \to T_\mu)$ methods is significant for the S_E soil profile at $T \cong 0.5$ s ($\gamma \cong 0.2$ for $R = 6$ and 8). Thus, it is evident that scaling ground motions based on spectral intensity measures (i.e., $S_a(T_o)$ and $S_a(T_o \to T_\mu)$) is not necessarily effective for all structural strength levels, period ranges, and site soil characteristics. This finding is reinforced using results from the MDOF analyses later in the paper.

Effect of epicentral distance on scatter

Figure 14 shows the COV-spectra for the scatter in Δ_{nlin} using the SAC design level S_D soil NF ground motion ensemble for the EP hysteresis type with $\alpha = 0.10$. Based on Figures 8 and 14, the NF ensemble tends to exhibit less or similar scatter as compared to the far-field ensemble for the $\overline{PGA}$, $\overline{EPA}$, and $\bar{A}_{95}$ methods. The dependency of the scatter for these scaling methods on the period is significantly smaller for the near-field ensemble. Figure 14(a) shows that the $\overline{EPA}$ method results in larger scatter than the $\overline{PGA}$ method, except for short-period structures with small R. The differences between the $\bar{A}_{95}$ method and the $\overline{PGA}$ method are negligible, except for $T < \sim 0.5$ s (Figure 14(b)).

The $\overline{PGA}$ method is compared to the $\overline{EPV}$ method in Figure 14(c) and to the $\overline{MIV}$ method in Figure 14(d). The effectiveness of both methods as compared to the $\overline{PGA}$ method is highly dependent on T and R. The $\overline{MIV}$ method is modestly more effective in reducing scatter for larger R ratios in shorter period ranges ($T < \sim 0.75$ s) and for smaller R ratios in longer period ranges ($T > \sim 0.8$ s).

The $\overline{PGA}$ method is compared to the $\bar{S}_a(T_o)$ and $\bar{S}_a(T_o \to T_\mu)$ methods in Figures 14(e) and (f), respectively. As compared to the far-field records in Figures 8(e) and (f), the effectiveness of both methods with respect to the $\overline{PGA}$ method is significantly decreased for the entire period range for $R \geqslant 2$, especially for larger values of R. Except for long periods and small R, the $\bar{S}_a(T_o)$ method is less effective or only slightly more effective than the $\overline{PGA}$ method. As compared to the $\bar{S}_a(T_o)$ method, the scatter for the $\bar{S}_a(T_o \to T_\mu)$ method is reduced, especially for larger R. The dependency of scatter on R using both methods is noticeable.

Figure 9(d) shows that the $\overline{MIV}$ method is more effective than the $\bar{S}_a(T_o)$ method in reducing scatter for $\sim 0.15 < T < \sim 1.05$ s with $R = 6$ and 8 for the SAC NF ground motion ensemble. The $\overline{MIV}$ method does not provide any significant improvement as compared to the $\bar{S}_a(T_o \to T_\mu)$ method.

Results for the MDOF frame structures

As discussed above, the $\overline{MIV}$ method provides better reduction in scatter than the $\bar{S}_a(T_o)$ and $\bar{S}_a(T_o \to T_\mu)$ methods for a significant range of structural periods, especially for soft (S_E) soil

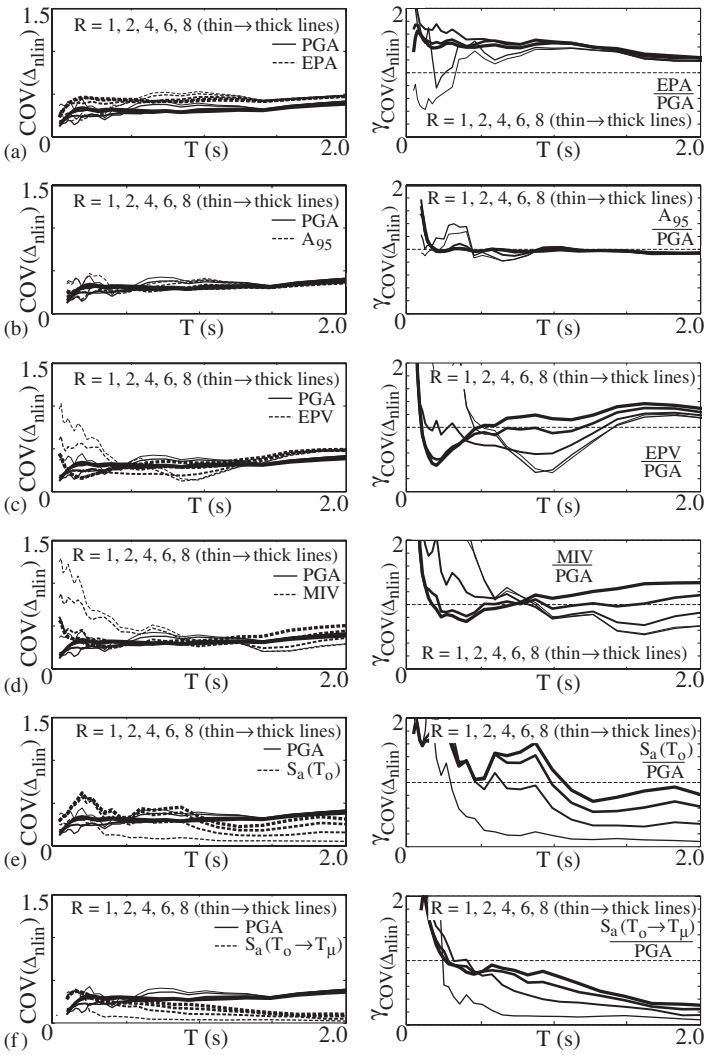

Figure 14. Scatter in Δ_{nlin} for the SAC NF ensemble (EP type, $\alpha = 0.10$)—$\overline{PGA}$ method compared to: (a) $\overline{EPA}$; (b) $\bar{A}_{95}$; (c) $\overline{EPV}$; (d) $\overline{MIV}$; (e) $\bar{S}_a(T_o)$; (f) $\bar{S}_a(T_o \to T_\mu)$ methods.

ground motion ensembles and for large R ratios. This may be because, the $\overline{MIV}$ method is able to capture the impulsive characteristics typical of ground motions recorded on soft soil profiles. To show that the results obtained from the SDOF analyses are applicable to MDOF systems, the scatter in the lateral displacements of the four-story and eight-story structures described earlier is investigated below.

Figure 15 shows the peak floor/roof lateral displacement demand, Δ_i, and interstory drift demand, θ_i, scatter profiles for the four-story and eight-story structures subjected to the UND S_E soil ground motion ensemble. The peak lateral displacement, Δ_i, values are normalized

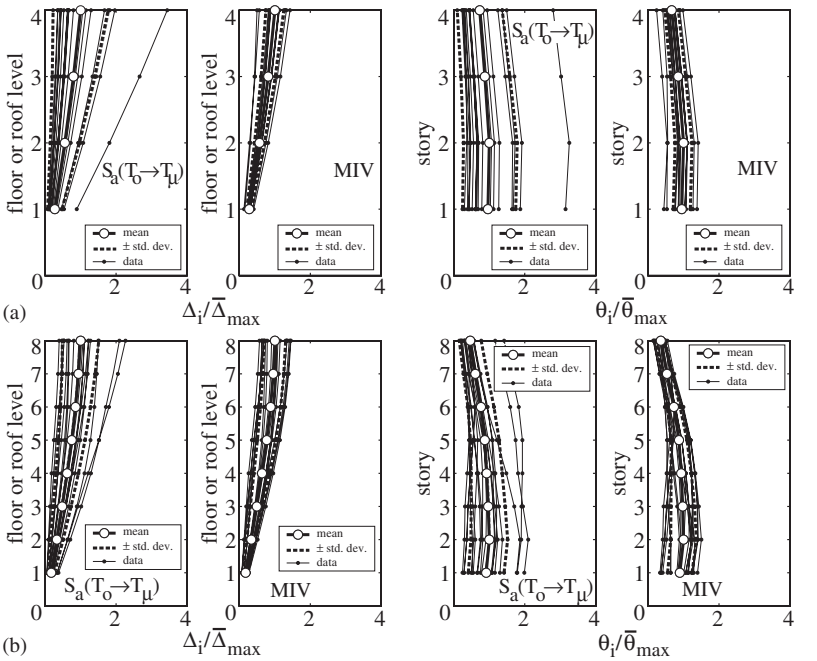

Figure 15. Scatter in MDOF demands for the UND S_E soil ensemble—$\overline{MIV}$ method compared to $\bar{S}_a(T_o \rightarrow T_\mu)$ method: (a) four-story frame; (b) eight-story frame.

with the maximum mean floor/roof displacement demand, $\bar{\Delta}_{max}$, calculated by taking the mean peak displacement demand at each floor and roof level and then taking the maximum value of the mean peak displacement demands over the height of the structure. Similarly, the peak interstory drift, θ_i, values are normalized with the maximum mean interstory drift demand, $\bar{\theta}_{max}$, calculated by taking the mean peak interstory drift demand in each story and then taking the maximum value of the mean peak interstory drift demands over the height. It is evident from the narrow ± standard deviation, σ, bands that, in each case, the $\overline{MIV}$ method provides a significant reduction in scatter as compared to the $\bar{S}_a(T_o \rightarrow T_\mu)$ method. This observation is more apparent for the four-story structure (Figure 15(a)). Based on the SDOF results shown previously, the reduction in scatter as compared to the $\bar{S}_a(T_o)$ method is expected to be more significant; however, this was not investigated for the MDOF structures.

Figure 16 shows the peak floor/roof displacement, Δ_i, and interstory drift, θ_i, COV profiles for the four-story and eight-story structures. The results display similar trends as the corresponding normalized peak displacement and interstory drift profiles in Figure 15, and compare reasonably well with the COV values for the SDOF models at $T_o = 0.49$ and 0.87 s (i.e., the fundamental periods of the four-story and eight-story structures), respectively, in Figures 13(d) and (f). Thus, the results from the MDOF analyses support the results from the SDOF analyses.

Note that the observations made above for the scatter in the peak floor/roof lateral displacement, Δ_i, and interstory drift, θ_i, demands are also applicable for the scatter in the peak

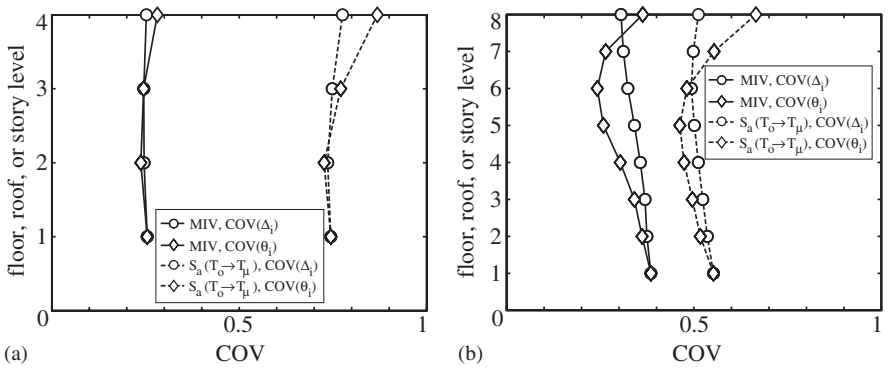

Figure 16. Coefficient of variation in the MDOF demands for the UND S_E soil ensemble—$\overline{MIV}$ method compared to $\bar{S}_a(T_o \rightarrow T_\mu)$ method: (a) four-story frame; (b) eight-story frame.

displacement ductility demand, μ. This is because, the structure lateral 'yield strength', and thus, the 'yield displacement' remain the same regardless of the ground motion used in each analysis. Thus, the scatter in μ is the same as the scatter in Δ (or θ) for the MDOF structures.

The scatter in the MDOF demand estimates in Figure 15 demonstrate that scaling ground motion records using methods that do not adequately represent the seismic intensity for the site conditions and structural characteristics considered can introduce a significant bias in the estimation of damage, unless a large number of records is used. Note that as the scatter in Δ, θ, and μ increase, the scatter in other demand indices (e.g., cumulative plastic deformation, residual displacement, number of yield reversals) are also expected to increase. Thus, reducing the scatter in Δ, θ, and μ is important for seismic design approaches that use multiple demand indices, as described by Farrow and Kurama [9, 46].

The reduced scatter in the seismic demands using the $\overline{MIV}$ method, together with its simplicity, make the $\overline{MIV}$ method advantageous over the other scaling methods described herein for a wide range of site and structure characteristics. The advantages of the $\overline{MIV}$ method over the $\bar{S}_a(T_o)$ and $\bar{S}_o(T_o \rightarrow T_\mu)$ methods come from: (1) the $\overline{MIV}$ method is based only on ground motion parameters and not on structural parameters (e.g., structural period, T_o), which may not be known in advance; and (2) ground motions scaled using the $\overline{MIV}$ method can be used to analyze structures with different properties (e.g., different T_o). Thus, it is recommended that for the period ranges shown in Figure 9, non-linear dynamic analyses of structures that are designed to undergo large non-linear displacements (i.e., with large R ratios) are conducted using ground motion records scaled based on the $\overline{MIV}$ method, particularly for soft soil profiles.

The biggest disadvantage for the implementation of the $\overline{MIV}$ scaling method in current seismic design procedures is the lack of methods to estimate the mean annual frequency of exceedence of MIV and methods to estimate the attenuation of MIV. Thus, there is currently no accepted method to determine the probability of exceedence of a certain MIV level at a given site. Future research is needed in these areas before the $\overline{MIV}$ scaling method can be used in practice.

CONCLUSIONS AND RECOMMENDATIONS

This paper investigates the effectiveness of seven ground motion scaling methods in reducing the scatter in peak lateral displacement demand estimates from non-linear dynamic time-history analyses. A series of single-degree-of-freedom (SDOF) and multi-degree-of-freedom (MDOF) structures are considered, including the effect of site soil characteristics, epicentral distance, structure yield strength, structure period, and hysteretic behavior. The main conclusions are as follows:

1. For the very dense (S_C), stiff (S_D), and soft (S_E) soil ground motion ensembles at long periods, the $\overline{MIV}$ method is more effective in reducing the scatter in the peak displacement demand than the $\overline{PGA}$ method. For shorter periods, the effectiveness of the $\overline{MIV}$ method decreases as the strength ratio, R decreases.

2. For the S_C and S_D soil ground motion ensembles, the $\bar{S}_a(T_o)$ method is significantly more effective in reducing the scatter than the $\overline{PGA}$ method, except for short- and very short-period structures. The effectiveness of the $\bar{S}_a(T_o)$ method decreases as R increases.

3. Since the $\bar{S}_a(T_o \rightarrow T_\mu)$ method accounts for the non-linear behavior expected in the structure, the scatter using this scaling method is smaller than the scatter using the $\bar{S}_a(T_o)$ method, particularly for larger R. However, the differences between the two methods are usually not very large.

4. The scatter in the peak displacement demand, Δ_{nlin}, and the peak displacement ductility demand, μ, are not significantly affected by the hysteretic behavior of the structure.

5. For the S_C, S_D, and S_E soil ground motion ensembles, the $\overline{MIV}$ method is more effective in reducing the scatter in the peak displacement demand than the $\bar{S}_a(T_o)$ and $\bar{S}_a(T_o \rightarrow T_\mu)$ methods for a wide range of periods with larger R ratios (especially with $R > 6$). The reduction in the scatter when using the $\overline{MIV}$ method is particularly significant for the S_E soil ensemble. Thus, it is concluded that scaling ground motion records based on spectral intensity measures (i.e., $S_a(T_o)$ and $S_a(T_o \rightarrow T_\mu)$) is not necessarily effective for all site soil characteristics, structure lateral strengths, and periods.

6. For the S_E soil and near-field (NF) ground motion ensembles, the effectiveness of the $\bar{S}_a(T_o)$ and $\bar{S}_a(T_o \rightarrow T_\mu)$ methods with respect to the $\overline{PGA}$ method is significantly decreased. Except for long periods, the $\bar{S}_a(T_o)$ and $\bar{S}_a(T_o \rightarrow T_\mu)$ methods are less effective than the $\overline{PGA}$ method for the S_E soil ensemble. For the NF ground motion ensemble, the effectiveness of the $\bar{S}_a(T_o)$ and $\bar{S}_a(T_o \rightarrow T_\mu)$ methods in the long period range decreases as R increases.

7. In general, the dependency of the scatter in the peak displacement demand on R is larger for the NF and S_E soil ground motion ensembles than for the S_C and S_D soil ensembles.

8. For the $\overline{PGA}$, $\overline{EPA}$, and $\bar{A}_{95}$ scaling methods, the dependency of the scatter in the peak displacement demand on the period T is significantly decreased for the near-field (NF) ground motion ensemble.

9. The coefficient of variation, COV, values for the scatter in the peak lateral displacements of the MDOF four-story and eight-story structures using the $\overline{MIV}$ and $\bar{S}_a(T_o \rightarrow T_\mu)$ scaling methods compare reasonably well with the corresponding COV values from the SDOF models. Thus, the results from the MDOF analyses support the results from the SDOF analyses.

10. The reduced scatter in the seismic demands using the $\overline{MIV}$ method, together with its simplicity, make the $\overline{MIV}$ method advantageous over the other scaling methods considered in this paper for a wide range of site and structure characteristics. It is recommended that for the period ranges given in the paper, non-linear dynamic analyses of structures that are designed to

undergo large non-linear displacements (i.e., with large R ratios) are conducted using ground motion records scaled based on the $\overline{MIV}$ method, particularly for soft soil profiles.

11. The biggest disadvantage for the implementation of the $\overline{MIV}$ scaling method in current seismic design procedures is the lack of methods to estimate the mean annual frequency of exceedence of MIV and methods to estimate the attenuation of MIV. Thus, there is currently no accepted method to determine the probability of exceedence of a certain MIV level at a given site. Future research is needed in these areas before the $\overline{MIV}$ scaling method can be used in practice.

12. The scatter in the ductility demand, μ, in terms of the sample standard deviation, σ, increases as R increases. The scatter in μ in terms of the coefficient of variation, COV (which normalizes σ by the sample mean), does not increase with R as much as the increase in terms of σ.

13. The scatter in μ does not depend on the scaling method when the structure yield strength, $F_y = F_{elas}/R$, is recalculated based on the acceleration response spectra of each ground motion used in an ensemble.

ACKNOWLEDGEMENTS

This research is funded by the National Science Foundation (NSF) under Grant No. CMS 98-74872 as part of the CAREER Program. The support of the NSF Program Directors Dr S.C. Liu and Dr P. Chang is gratefully acknowledged. The opinions, findings, and conclusions expressed in the paper are those of the authors and do not necessarily reflect the views of the NSF or the program directors acknowledged above.

REFERENCES

1. International Code Council (ICC). International Building Code (IBC), Falls Church, VA, 2000.
2. International Council of Building Officials (ICBO). Uniform Building Code, Whittier, CA, 1997.
3. American Society of Civil Engineers (ASCE). Prestandard and Commentary for the Seismic Rehabilitation of Buildings, FEMA 356, Federal Emergency Management Agency, Washington, D.C., 2000.
4. Shome N, Cornell C. Normalization and scaling accelerograms for nonlinear structural analysis. *Sixth U.S. National Conference on Earthquake Engineering*, Seattle, WA, 1998 (CD-ROM).
5. Vidic T, Fajfar P, Fischinger M. Consistent inelastic design spectra: strength and displacement. *Earthquake Engineering and Structural Dynamics* 1994; **23**:507–521.
6. Miranda E. Site-dependent strength-reduction factors. *Journal of Structural Engineering* (ASCE) 1993; **119**: 3503–3519.
7. Nau J, Hall W. Scaling methods for earthquake response spectra. *Journal of Structural Engineering* (ASCE) 1984; **110**: 91–109.
8. Lam N, Wilson J, Hutchinson G. The ductility reduction factor in the seismic design of buildings. *Earthquake Engineering and Structural Dynamics* 1998; **27**:749–769.
9. Farrow KT, Kurama Y. Capacity-Demand Index Relationships for Performance-Based Seismic Design. Structural Engineering Research Report #NDSE-01-02, Department of Civil Engineering and Geological Sciences, University of Notre Dame, Notre Dame, IN, 2001. http://www.nd.edu/∼concrete
10. Shome N, Cornell C, Bazzurro P, Carballo J. Earthquakes, records, and nonlinear responses. *Earthquake Spectra* 1998; **14**:469–500.
11. Martinez-Rueda J. Scaling procedure for natural accelerograms based on a system of spectrum intensity scales. *Earthquake Spectra* 1998; **14**:135–152.
12. Nassar A, Krawinkler H. Seismic Demands for SDOF and MDOF Systems. John A. Blume Earthquake Engineering Center, Report No. 95, Dept. of Civil Engineering, Stanford University, Stanford, CA, 1991.
13. Kennedy R, Short S, Merz K, Tokarz F, Idriss I, Powers M, Sadigh K. Engineering Characterization of Ground Motion-Task I: Effects of Characteristics of Free-Field Motion on Structural Response. NUREG/CR-3805, U.S. Regulatory Commission, Washington, D.C., 1984.

14. Arias A. A Measure of Earthquake Intensity. Seismic Design of Nuclear Power Plants, The Massachusetts Institute of Technology, Cambridge Press, 1969.
15. Riddell R, Newmark NM. Statistical Analysis of the Response of Nonlinear Systems Subjected to Earthquakes. UILU-ENG 79-2016, Structural Research Series, Dept. of Civil Engineering, Univ. of Illinois, Urbana, IL, 1979.
16. Trifunac MD, Lee VW. Empirical models for scaling pseudo relative velocity spectra of strong earthquake accelerations in terms of magnitude, distance, site intensity and recording site conditions. *Soil Dynamics and Earthquake Engineering* 1989; **8**:126–144.
17. Trifunac MD. Scaling earthquake motions in geotechnical design. *Third International Conference on Recent Advances in Geotechnical Earthquake Engineering and Soil Dynamics*, University of Missouri-Rolla, Rolla, MO, 1995; **II**: 607–612.
18. Cornell CA, Luco N. Ground motion intensity measures for structural performance assessment at near-fault sites. *U.S.–Japan Joint Workshop and Third Grantees Meeting*, U.S.–Japan Cooperative Research on Urban Earthquake Disaster Mitigation, University of Washington, Seattle, WA, 2001.
19. Carballo JE, Cornell CA. Input to nonlinear structural analysis; modification of available accelerograms for different source and site characteristics. *Sixth U.S. National Conference on Earthquake Engineering*, Seattle, WA, 1998 (CD-ROM).
20. Keaton JR, Zeng Y, Anderson JG. Procedure for scaling earthquake records to match acceleration response spectra for engineering design. *Sixth International Conference on Seismic Zonation: Managing Earthquake Risk in the 21st Century*, EERI, Palm Springs, CA, 2000 (CD-ROM).
21. Carballo JE. Probabilistic Seismic Demand Analysis; Spectrum Matching and Design. Ph.D. Dissertation and Report RMS-41, Stanford Univ., Stanford, CA, 2000. http://pitch.stanford.edu/rmsweb/Reports/RMS41.pdf
22. Cordova PP, Deierlein GG, Mehanny SF, Cornell CA. Development of a two parameter seismic intensity measure for probabilistic assessment procedure. *Second U.S.–Japan Workshop on Performance-Based Earthquake Engineering Methodology for Reinforced Concrete Building Structures*, Sapporo, Japan, 2000, PEER Center, University of California, Berkeley, CA; 195–214.
23. Luco N. Probabilistic Seismic Demand Analysis, SMRF Connection Fractures, and Near-source Effects. Ph.D. Dissertation, Stanford University, Stanford, CA, 2001.
24. Vamvatsikos D, Cornell CA. Incremental Dynamic Analysis: Theory and Applications in Earthquake Engineering. Report No. RMS-46, RMS Program, Stanford University, Stanford, CA, 2002.
25. Mahin SA, Bertero VV. An Evaluation of Some Methods for Predicting the Seismic Behavior of Reinforced Concrete Buildings. UCB/EERC-75-5, Earthquake Engineering Research Center, University of California, Berkeley, CA, 1975.
26. Kurama Y. Simplified seismic design approach for friction-damped unbonded post-tensioned precast walls. *ACI Structural Journal* 2001; **98**:705–716.
27. Paulay P, Priestley M. *Seismic Design of Reinforced Concrete and Masonry Buildings*. Wiley: New York, NY, 1992.
28. Prakash V, Powell G, Campbell S. DRAIN-2DX Base Program Description and User Guide: Version 1.10. Report No. UBC/SEMM-93/17, Department of Civil Engineering, University of California, Berkeley, CA, 1993.
29. Wu S. Seismic Analysis and Retrofit of Non-Ductile Reinforced Concrete Frame Buildings. Ph.D. Dissertation, Dept. of Civil and Environmental. Eng., Lehigh University, Bethlehem, PA, 1995.
30. Somerville P, Smith N, Punyamurthula S, Sun J. Development of Ground Motion Time Histories for Phase 2 of the FEMA/SAC Steel Project. Report No. SAC/BD-97/04, SAC Joint Venture, Sacramento, CA, 1997.
31. Kurama Y, Sause R, Pessiki S, Lu LW. Seismic Design and Response Evaluation of Unbonded Post-Tensioned Precast Concrete Walls. Research Report No. EQ-97-01, Department of Civil and Environmental Engineering, Lehigh University, Bethlehem, PA, 1997.
32. McCann M, Shah H. Determining strong-motion duration of earthquakes. *Bulletin of the Seismological Society of America* 1979; **69**:1253–1265.
33. Federal Emergency Management Agency (FEMA). NEHRP Recommended Provisions for the Development of Seismic Regulations for New Buildings. Volumes 1 and 2, Washington, D.C., 1994.
34. Applied Technology Council (ATC). Tentative Provisions for the Development of Seismic Regulations for Buildings. ATC 3-06, 1978.
35. Sarma SK, Yang KS. An evaluation of strong motion records and a new parameter A_{95}. *Earthquake Engineering and Structural Dynamics* 1987; **15**:119–132.
36. Anderson JC, Bertero VV. Uncertainties in establishing design earthquakes. *Journal of Structural Engineering* (ASCE) 1987; **113**:1709–1724.
37. Decanini LD, Mollaioli F. Parameters to be considered in the establishment of the design earthquake based on energy concepts. *Structural Engin. World Wide*, Paper T227-5, Elsevier, 1998.
38. Naeim F, Anderson JC. Classification and Evaluation of Earthquake Records for Design. CE 93-08, Dept. of Civil Engineering, Univ. of Southern California, Los Angeles, CA, 1993.
39. Naeim F, Anderson JC, Jain S. A data base of earthquake records for design. *Fifth U.S. National Conference on Earthquake Engineering*, Oakland, CA, 1994; **II**: 263–272.

40. Krawinkler H, Rahnama M. Effects of soft soil on design spectra. *Tenth World Conference on Earthquake Engineering*, Madrid, Spain, 1992; 5841–5846.
41. The Math Works, Inc. MATLAB. Natick, MA, 2000.
42. Farrow KT, CDSPEC. WWW Document, http://www.nd.edu/∼concrete, December 2001.
43. Clough R, Penzien J. *Dynamics of Structures.* (2nd edn). McGraw-Hill: New York, NY, 1993.
44. Chopra A, Goel R. Capacity-demand-diagram methods based on inelastic demand spectrum. *Earthquake Spectra* 1999; **15**:637–656.
45. Freeman SA. Development and use of capacity demand spectrum method. *Sixth U.S. National Conference on Earthquake Engineering*, Seattle, WA, 1988 (CD-ROM).
46. Farrow KT, Kurama Y. SDOF demand index relationships for performance-based seismic design. *Earthquake Spectra* 2003; **19**: to appear.

